



A 3D forward stratigraphic model of fluvial meander-bend evolution for prediction of point-bar lithofacies architecture

Na Yan*, Nigel P. Mountney, Luca Colombera, Robert M. Dorrell

Fluvial & Eolian Research Group, School of Earth and Environment, University of Leeds, UK

ARTICLE INFO

Keywords:

Fluvial meander
Point bar
Counter-point bar
Forward stratigraphic model
Sedimentology

ABSTRACT

Although fundamental types of fluvial meander-bend transformations – expansion, translation, rotation, and combinations thereof – are widely recognised, the relationship between the migratory behaviour of a meander bend, and its resultant accumulated sedimentary architecture and lithofacies distribution remains relatively poorly understood. Three-dimensional data from both currently active fluvial systems and from ancient preserved successions known from outcrop and subsurface settings are limited. To tackle this problem, a 3D numerical forward stratigraphic model – the *Point-Bar Sedimentary Architecture Numerical Deduction (PB-SAND)* – has been devised as a tool for the reconstruction and prediction of the complex spatio-temporal migratory evolution of fluvial meanders, their generated bar forms and the associated lithofacies distributions that accumulate as heterogeneous fluvial successions. PB-SAND uses a dominantly geometric modelling approach supplemented by process-based and stochastic model components, and is constrained by quantified sedimentological data derived from modern point bars or ancient successions that represent suitable analogues. The model predicts the internal architecture and geometry of fluvial point-bar elements in three dimensions. The model is applied to predict the sedimentary lithofacies architecture of ancient preserved point-bar and counter-point-bar deposits of the middle Jurassic Scalby Formation (North Yorkshire, UK) to demonstrate the predictive capabilities of PB-SAND in modelling 3D architectures of different types of meander-bend transformations. PB-SAND serves as a practical tool with which to predict heterogeneity in subsurface hydrocarbon reservoirs and water aquifers.

1. Introduction

Fluvial meander bends and their associated deposits record the transformation of a river's position across its floodplain over time (Nanson and Croke, 1992). Several fundamental types of transformations are recognised: expansion, translation, rotation, and combinations thereof (see Fig. 1, Brice, 1974; Daniel, 1971; Ghinassi et al., 2014; Jackson, 1976; Makaske and Weerts, 2005). However, relationships between the migratory behaviour of a river, the geometry of accumulated sedimentary bodies (e.g., point bars, counter-point bars) that arise from channel migration, and the resultant internal lithofacies distribution within these bodies remain relatively poorly understood (Hooke and Yorke, 2011; Nanson and Hickin, 1983; Nicoll and Hickin, 2010; Smith et al., 2009; Thomas et al., 1987). In present-day meandering fluvial systems, the planform morphologies of point bars and their relationship to formative channel reaches are evident but subsurface lithofacies distributions are typically only poorly revealed by localised river cuts, by shallow borehole data that essentially provide

only 1D sections, or by geophysical investigations such as ground penetrating radar surveys that provide higher resolution 2D cross sections but which are usually limited to shallow depth (Bridge et al., 1995; Kostic and Aigner, 2007; Labrecque et al., 2011; Miall, 1994; Musial et al., 2012). By contrast, although ancient outcrop successions reveal vertical and lateral relationships between accumulated lithofacies, these successions cannot usually be directly related to the original planform morphologies of the preserved point-bar elements in which they are contained. A small number of exceptional outcrops expose both vertical and horizontal sections (e.g., Edwards et al., 1983; Foix et al., 2012; Smith, 1987), but even these are fragmentary 'windows' that reveal only a minor part of large and complex 3D geological bodies.

Overall, our ability to unequivocally reconstruct the complex spatio-temporal evolutionary history and internal architecture of meander bends and their deposits remains limited (Bridge, 2003; Miall, 1996; Colombera et al., 2017).

Recent developments of numerical modelling approaches have

* Corresponding author.

E-mail address: n.yan@leeds.ac.uk (N. Yan).

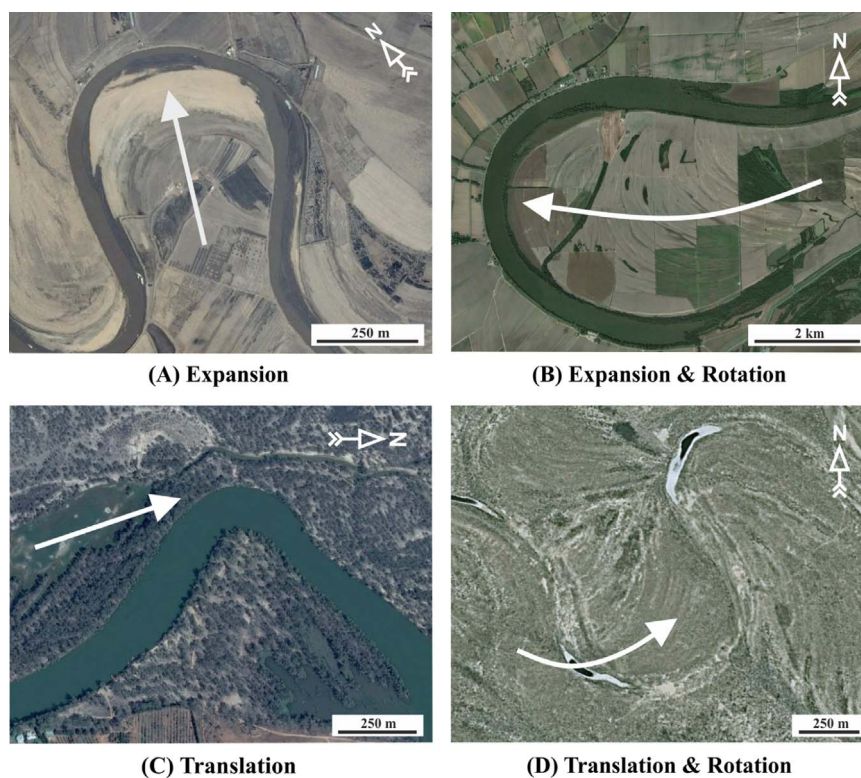


Fig. 1. Four basic types of meander-bend transformations (see Ghinassi et al., 2014). The arrows show the migration direction of meander bends. Examples from modern rivers (Google Earth™): (A) Songhua River, China (46°38' N, 126°30' E); (B) Mississippi River, USA (34°25' N, 90°46' W); (C) Murray River, Australia (34°14' S, 142°15' E); (D) Rio Negro, Argentina (39°49' S, 64°56' W).

provided a significant contribution to these reconstructions (e.g., Hassanpour et al., 2013). Here, we present and utilise the *Point-Bar Sedimentary Architecture Numerical Deduction* (PB-SAND), which uses a primarily geometric-based modelling approach that is supported by process- and stochastic-based methods, coded in Matlab and C#, to reconstruct and predict the complex spatio-temporal evolution of a variety of meandering river behaviours in detail. Specifically, the model seeks to predict variations in 3D geometry and lithofacies distribution of sand- and mud-prone packages that accumulate as fluvial meander deposits in response to different conditions of channel migration.

Specific research objectives of this study are as follows: (1) to demonstrate how PB-SAND can serve as a tool to help understand potential relationships between evolutionary trajectories and lithofacies distributions of fluvial meandering systems and their preserved deposits; (2) to apply the model to predict the relationship between fluvial expansional point-bar and downstream-translating bar geometries, and internal lithofacies distributions, in a selected case study from the stratigraphic record; (3) to demonstrate possible scenarios of meander evolution, cut-off and preservation; (4) to show how the model improves our ability to reproduce stratigraphic complexity and heterogeneity in fluvial depositional systems at different temporal and spatial scales in 3D; and (5) to illustrate how the modelling approach is directly applicable to palaeo-environmental reconstruction, and to subsurface hydrocarbon reservoir and groundwater aquifer appraisal.

2. Modelling algorithms

Since the pioneering work of Fisk (1944) on the characterisation of meanders of the Mississippi River, many studies have attempted to understand how flow dynamics, sediment transport, cut-bank erosion, and channel geometry interact to collectively control meander migration, resultant point-bar development, and the distribution of lithofa-

cies within such sedimentary bodies (Jackson, 1976; Musial et al., 2012; Nicoll and Hickin, 2010; Schumm, 1960; Walker, 2006; Willis and Tang, 2010). Nonetheless, this remains challenging due to the complex interplay between the power of a stream to transport sediment and the resistance of cut banks to erosion, further complicated by a variety of inherited antecedent conditions, including substrate and vegetation type and distribution (Hickin, 1984; Motta et al., 2012; Nanson and Croke, 1992). Process-based models that use empirical equations and hydro-morphological relations have inherent limitations due to the complexity of channel patterns in natural streams; these models typically demand high computational resources (Brownlie, 1983; Leeder, 1973; Schumm, 1960). Consequently, we employ a primarily geometric-based modelling approach, supported by stochastic- and process-based techniques to model fluvial meander and bar development. The geometric modelling approach is grid-free and vector-based; it is well suited to the simulation of lithological heterogeneity at multiple spatial scales. A similar geometric approach by Hassanpour et al. (2013) is able to model the distribution of mud drapes in expansional point bars for early-stage development without neck cut-off. The PB-SAND model developed here can additionally model: (1) different meander-bend transformation behaviours; (2) complex spatial heterogeneity distributions of facies associations arising from different growth behaviours; (3) complex nested sets of bar-front mud drapes that typically arise in response to multiple processes that operate on different time scales; and (4) variations of facies within each inclined bar accretion element (scroll-bar unit).

The approach requires definition of several fundamental parameters, including type of meander-bend transformation, sinuosity, stream-wise distance away from meander apex, and position of inflection points of a meander loop; see details in the following sections. In this study, model inputs to constrain channel-form and bar geometries have been acquired from field-based measurements of

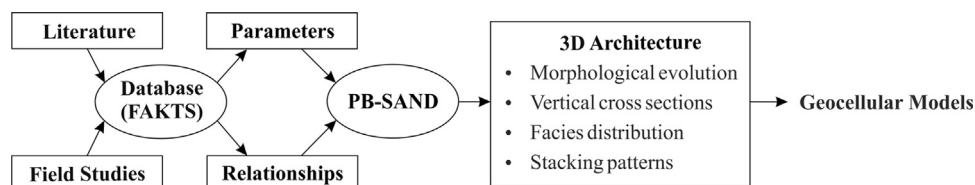


Fig. 2. Flow diagram of the modelling strategy. Detailed inputs and outputs can be found in Fig. A.1.

outcrops and modern systems, from remote sensing imagery, and from subsurface data (e.g., seismic, cores and well logs). Data that describe such real-world examples are held in the Fluvial Architecture Knowledge Transfer System (FAKTS) – a relational database that stores quantified sedimentological data from many modern classified fluvial systems and analogue ancient fluvial successions (see details in Colomera et al., 2012, 2013, 2017), which is populated with sedimentological data from the published literature and our own field studies.

The modelling work-flow is illustrated in Fig. 2; examples of FAKTS outputs that are used to parameterise the model are shown in Fig. 3. The modelling approach, including the ability to incorporate and use FAKTS-hosted data from multiple real-world examples as inputs to PB-SAND, brings several advantages: (1) flexibility to determine meander-bend migration rates and morphology without the need to account for complicated hydraulic processes; (2) capability to incorporate independent geomorphic controls (e.g., valley confinement); (3) ability to constrain the model output using parameters derived directly from empirical field measurements and remote sensing; (4) ability to directly compare modelling outcome with real-world datasets derived from outcrops, aerial imagery or subsurface data; and (5) high computational efficiency.

The following sections introduce the main modelling components of PB-SAND: (1) the novel algorithm developed to model morphological evolution of different types of meander-bend transformations in plan-view (cf. Ghinassi et al., 2014); (2) the algorithm to construct internal architecture and geometry of vertical cross sections of point-bar elements; and (3) the algorithm to simulate lithofacies distributions within bar-form elements. This study focuses solely on modelling single point-bar elements in the subsurface. However, PB-SAND can also be employed to model multiple point-bar elements, channel belts, and the pattern of stacking of such elements in the accumulated sedimentary record. Such functionality will be the subject of future work.

2.1. Planform meander-bend transformations

The planform evolution of meanders is modelled by specifying channel positions (coordinates) at three key time instances that capture the shape of a meander from its initiation, through mid-life, to a state of maturity, and possible eventual abandonment due to, for example, neck cut-offs (cf. Constantine and Dunne, 2008). The algorithm of modelling point-bar evolution in plan view is illustrated with an example in Fig. 4. Input data that define the bar positions over time can be derived from real-world examples of point bars that preserve scroll-bar surfaces as a record of their growth trajectories, for instance, point-bar examples stored in the FAKTS database (Colomera et al., 2013). Data are smoothed with a Savitzky-Golay filter, which uses a polynomial to fit successive sub-sets of adjacent data points by the method of linear least squares to increase the ratio of signal to noise without substantially distorting the signal (Savitzky and Golay, 1964). Smoothed data are then reduced or extrapolated to a series of control points that defines the position of each scroll-bar. Each bar position is defined by connecting these control points as a series of straight-line segments for computational efficiency. Evolutionary trajectories (as represented by the modelled positions of successive scroll-bar surfaces) are then interpolated linearly based on specified migration rates

between the key times. Evolutionary trajectories may be extrapolated beyond the state at the final time by specifying a predictive migration rate. To mimic natural river systems, the model simulates the progressive reworking of deposits by cut-bank erosion, for example where a meander neck narrows in the latter stage of its evolution.

Several input parameters are required to initiate and control model behaviour, as determined from active meandering fluvial systems or, in some cases, preserved successions stored in FAKTS, including:

- (1) Coordinates of scroll-bar positions that control the transition of different stages of a meander bend (see scroll bars at key times t_1 , t_2 , and t_3 in Figs. 4 and 5), which can be acquired from topographic maps or remote sensing imagery;
- (2) Average migration rates that control the spacing of scroll bars between these times ($t_1 - t_2$ and $t_2 - t_3$);
- (3) The prediction time (beyond t_3) and the associated migration rate, which will typically be based on the timing of abandonment of river reaches, for example, through a neck cut-off as a river approaches its maximum sinuosity or through a chute cut-off or nodal avulsion determined by the maximum growth time of meanders (Constantine and Dunne, 2008; Hooke, 2003; Slingerland and Smith, 2004);
- (4) River channel width and depth in relation to meander size;
- (5) The minimum separation distance between two sections of a looped channel that acts to trigger neck cut-off events.

Examples of modelling outcome are presented in Fig. 5: plan-view morphologies of different meander-bend transformation types, including expansion, translation, rotation, and combinations thereof, can all be modelled effectively (see Fig. 1); the coordinates of simulated scroll-bar surfaces that act as a record of point-bar migratory trajectories are exported as ASCII format text files in temporal sequence. These data can be imported into other industry standard software applications, e.g., Schlumberger Petrel. Older point-bar deposits are progressively overprinted (i.e., eroded) by the later phases of point-bar development. For example, the point-bar deposits in Fig. 5(A & B) demonstrate partial reworking of earlier deposits associated with bar initiation by later deposits associated with bar maturity as the loop tightens. In Fig. 5(C), in particular, the scroll bar at t_1 has been completely reworked and overprinted by more recent evolution of the same point-bar element as it approaches maturity. Thus, the morphology and geometry of modelled point-bar elements developed through different styles of meander-bend transformations effectively mimic real-world behaviour (Fig. 5 and Video 1 [supplemental]).

Supplementary material related to this article can be found online at <http://dx.doi.org/10.1016/j.cageo.2017.04.012>.

2.2. Stratigraphic geometries

The stratigraphic complexity of point-bar architecture is modelled based on scroll-bar geometries and patterns generated from the plan-view model described above. Unlike grid-based models, which are restrictive in how vertical sections are constructed, PB-SAND is able to generate vertical sections in any orientation. In vertical section view, the shape of inclined point-bar accretion surfaces is modelled as a half-cosine wave to mimic the typical form of down-lap of such surfaces

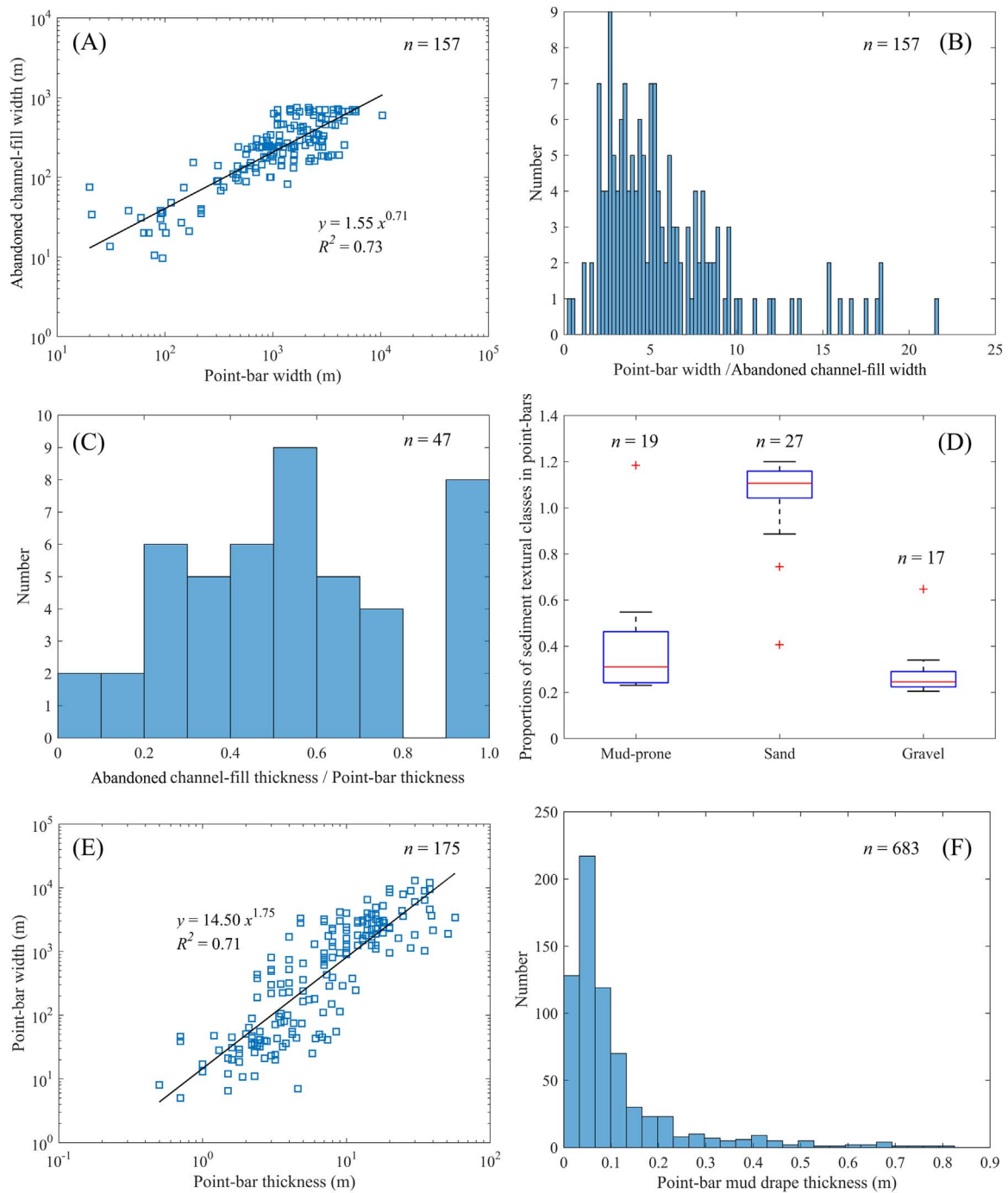


Fig. 3. Examples of data outputs from the FAKTS database that can be utilised to parameterise PB-SAND simulations. (A) Cross-plot of abandoned-channel-fill width vs. point-bar (or laterally accreting barforms) width, for pairs of adjacent architectural elements; data are from highest-quality FAKTS datasets only (so-called Data Quality Index [DQI] A, Colombera et al., 2012). (B) Distribution of the ratio between the width of point bars (or laterally accreting barforms) and adjacent abandoned-channel fills; highest-quality datasets only. (C) Distribution of the thickness ratio between laterally juxtaposed abandoned-channel fills and point bars (or laterally accreting barforms), on the basis of which the thickness of muddy deposits in channel fills can be set in PB-SAND. (D) Box-plots reporting the distribution in proportion of different facies grain-size classes in bars in FAKTS. (E) Cross-plot of point-bar (or laterally accreting barforms) width vs. thickness. (F) Distribution of the thickness of muddy facies units in laterally accreting barforms and adjacent abandoned-channel fills. See Colombera et al. (2017) for additional details.

onto channel bases and off-lap in the region where the upper part of the bar merges into floodplain (Fig. 6). The steepness and asymmetry of this cosine wave can be modified to simulate different types of bar-front geometries (cf. Rubin, 1987).

For cross sections perpendicular to the margin of a river channel, the shape of the inclined point-bar surfaces (i.e., wavelength) which typically dip from 1° to 25° (Miall, 1996) is dependent on the slope of the channel bank on the inner meander bend at the time of accumula-

tion; this is simulated by defining a channel width-depth ratio (cf. Wu et al., 2015). The resulting shape of inclined accretion surfaces is determined by how deposition occurs on the accreting part of a channel bend (Fig. 7). The standard wavelength of accretion surfaces $[\lambda, \text{m}]$ observed in cross-sections changes linearly with the migration rate of the bank, as is common in natural examples. The maximum wavelength $[\lambda_{max}, \text{m}]$ and minimum wavelength $[\lambda_{min}, \text{m}]$ are predefined wavelengths when the bank experiences the greatest erosion $[R_{dep}, \text{m yr}^{-1}]$

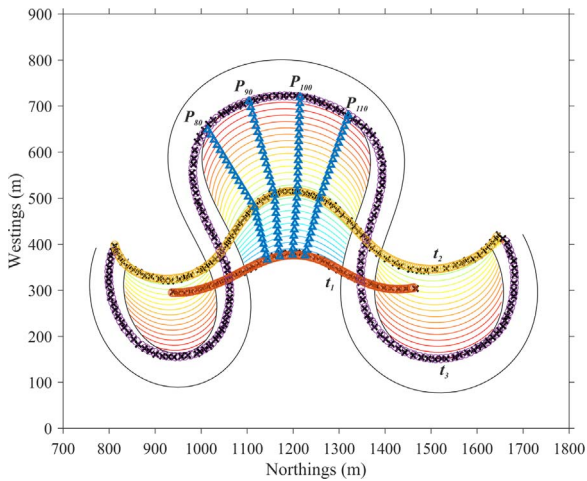


Fig. 4. An example of modelling point bar evolution in plan view. Black crosses denote input data at three key times ($n_{t1}=39$, $n_{t2}=73$, and $n_{t3}=154$). For each of these times, these data are then smoothed with a Savitzky-Golay filter that uses a polynomial order of 3 and a frame length of 21. Smoothed data are then extrapolated to control points (200 in this case) at each time, shown in red circles at t_1 , yellow circles at t_2 , and purple circles at t_3 , respectively. Bar positions between these key times are interpolated linearly. Trajectories of four representative points (P_{80} , P_{90} , P_{100} , and P_{110}) are shown in blue triangles. (For interpretation of the references to colour in this figure legend, the reader is referred to the web version of this article).

or deposition [R_{ero} , $m\ yr^{-1}$], respectively. Suitable values for wavelengths may be acquired from abandoned channel fills or active channel banks. The channel scour depth defines the thickness of the point-bar body being modelled. The dip of the inclined surfaces modelled within point-bar elements effectively mimics the true dip of real-world accretion surfaces with a gentle accretion slope at the inner bank and a steep erodible slope at the outer bank (cf. Dey, 2014). In a practical sense, the implementation of this algorithm allows the effective modelling of the shape of the river channel around a meander bend; modelled accreting channel banks closely match those observed in natural systems in terms of their asymmetry, mean slope, and change rate of these parameters around a river bend (cf. Carlston, 1965; Fielding and Crane, 1987; Leeder, 1973; Leopold and Wolman, 1960; Lorenz et al., 1985).

For vertical cross sections aligned obliquely to the margin of a river channel, the shape of inclined point-bar surfaces depicted is the apparent dip. This is modelled by projecting the vertical profiles of point-bar surfaces onto the plane of a cross section oriented obliquely to the growth direction of the point bar. Adjusted wavelengths [λ_a , m] of modelled accretion surfaces (Fig. 6) are calculated to account for the oblique trend relative to the propagation direction of the point bar at the time of accumulation: $\lambda_a = \lambda / \cos(\theta)$, where θ is the angle between the scroll-bar migration direction at a local-point and the direction of the oblique cross-section, for which the maximum angle permissible is specified as 89° , to avoid null division when θ is 90° .

As demonstrated in Fig. 6, the 2D architecture of cross sections can be rendered and depicted by specifying the start- and end-points of transects. The model can produce vertical profiles of cross-sectional

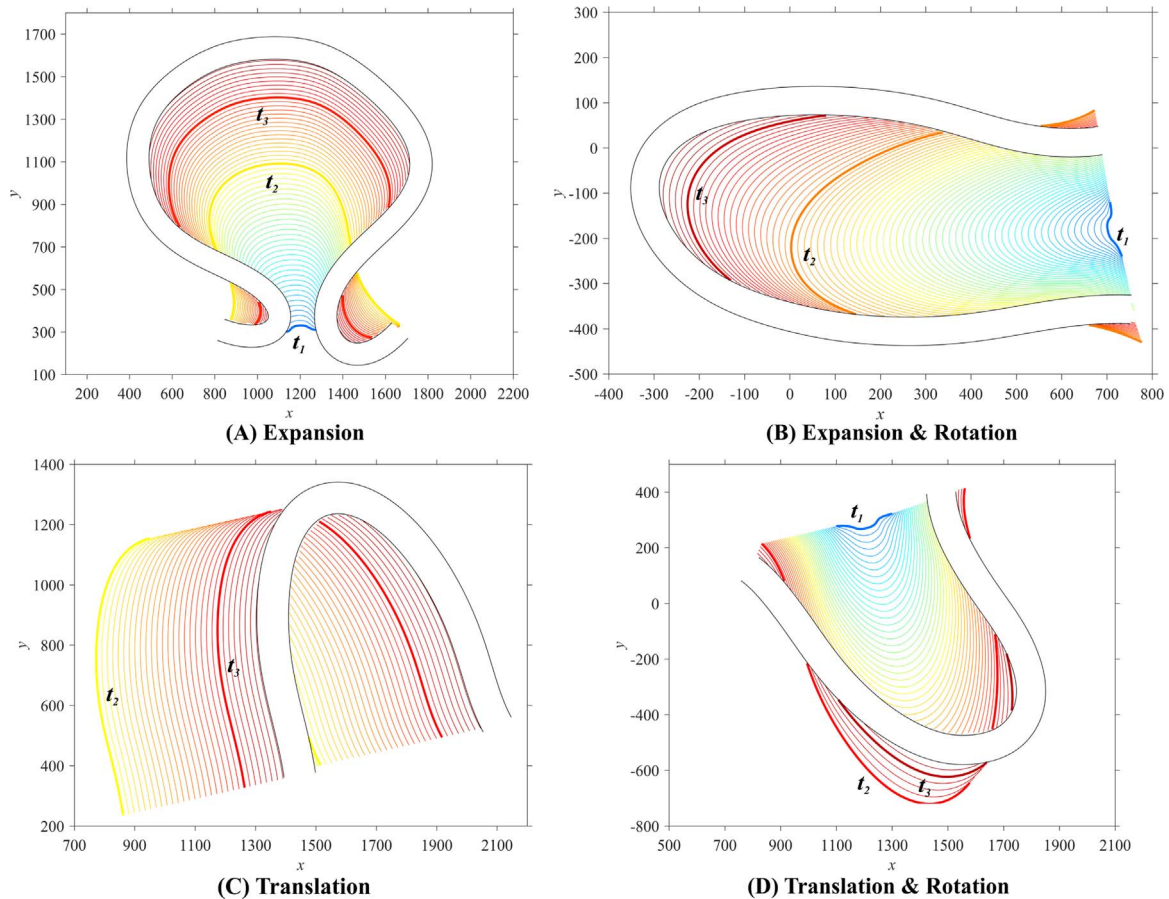


Fig. 5. Examples of modelling outputs showing four basic plan-form modes of meander-bend transformations. The temporal locations at t_1 , t_2 , and t_3 are shown in bold lines. A jet colour (dark blue to dark red) scheme is used to differentiate meander positions at different times. The dimension here is arbitrary, but the modelling results can be readily scaled to physical units by using data from field measurements or remote sensing. The shape of the modelled point bars is comparable with those found in the real world. (For interpretation of the references to colour in this figure legend, the reader is referred to the web version of this article).

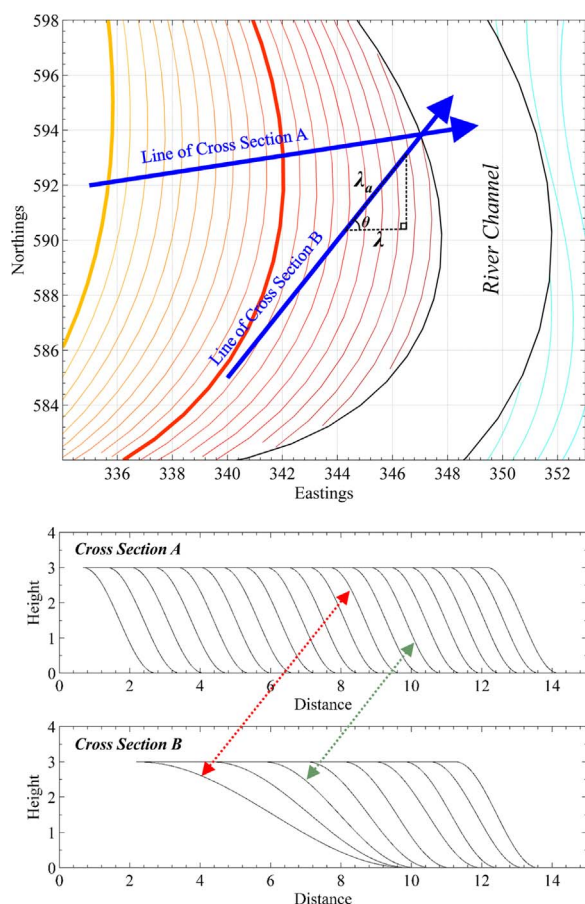


Fig. 6. Illustration of the method for calculating an adjusted wavelength of accretion surfaces. ‘Standard wavelength (λ)’ of the channel shape seen in cross-section A, which in its simplest form, is modelled as cosine-curve, the amplitude of which equates to half of the channel depth, and the wavelength of which equates to twice the width of each inclined accretion surface. This cosine-wave shape will be observable in a cross-section that passes through a point-bar element in an orientation perpendicular to the channel. ‘Adjusted wavelength (λ_a)’ of the channel body shape seen in cross-section B, which is an apparent measure of the ‘standard wavelength’ described above that accounts for the angle between the migration direction of a local-point and the direction of the cross-sectional slice. Note the gentler slopes of cross section B (apparent dips) in comparison to their counterparts of cross section A (true dips). (For interpretation of the references to colour in this figure legend, the reader is referred to the web version of this article).

slices in any orientation, including situations where a cross-section is tangential to a river bank or steps across the same reach multiple times.

2.3. Lithological characteristics

At its simplest, the migration of a meander bend arises from the erosion of the outer bank and the associated lateral accretion on the inner bank. This process, and associated helical river flow within the channel, favours the accumulation of a fining-upward vertical lithofacies succession composed of a suite of primary sedimentary structures that can be related to specific formative processes on different parts of the inner channel bank (Allen, 1970; Bridge, 1975; Jackson, 1976). Within the model, discrete lithofacies are assigned as an association that occurs in a predictable vertical succession. By default, a fining-upward succession is modelled. However, different lithofacies successions can be specified depending on the transformation types of point-bar elements being modelled, typically conditioned by data available in FAKTS. The proportion and distribution of these lithofacies is incorporated into the model as part of the accretion of point-bar architectural elements. The standard facies association may include, but is not limited to, the following lithology types: (a) gravel, (b) coarse sand, (c)

medium sand, (d) fine sand, (e) silt, and (f) clay-prone mud. Additional supplementary lithofacies types include the following: (g) mud that is deposited on accretion surfaces to form drapes during stages of low energy or slack water; (h) mud that accumulates in undisturbed floodplain areas between point-bar elements; and (j) conglomerate or breccia that accumulates in channel thalwegs as a result of localised reworking of bar fronts or outer-bend channel banks (e.g., intraformational mud-clast breccias) (Miall, 1996). The facies association may also additionally include specifications of petrophysical properties or particular sedimentary structures. The proportion and distribution of lithofacies is specified to model various types of bar forms that grow through different transformation behaviours.

Input parameters for modelling the facies organisation of bars can be derived from ancient or modern examples of point bars that represent suitable analogues to the deposits being modelled. Facies types, distributions and proportions within bar forms, as well as thickness of mud drapes and channel-thalweg gravels, are drawn from real-world case-study examples in FAKTS (Colombera et al., 2012, 2013). Spatial relationships between facies types, quantified in the form of transition statistics in FAKTS, can be employed to model vertical or lateral facies successions.

For packages of inclined strata in a point-bar element, lithofacies proportions are specified and defined as percentage of element thickness (Fig. 8). The heterogeneity of lithofacies associations, both spatially and temporally, is primarily determined by a set of rules that simulates the migration and evolution of meandering rivers. Five common ‘rule sets’ are defined and their respective algorithms are explained below. These rule sets are used to determine the spatio-temporal occurrence (proportion and distribution) of lithofacies within modelled point-bar elements, and can be applied individually or in combination. Additional rule sets can be devised to define lithofacies distributions associated with other types of meander development.

Rule set 1: Mud-prone areas associated with bend tightening. This mimics a situation in which the proportion of finer facies increases with meander-bend sinuosity (until abandonment or avulsion) due to a decline of flow energy caused by a higher degree of energy dissipation around the bend, as observed in rivers and outcrop analogues (Durkin, 2016; Hickin, 1974; Miall, 1996; Piet, 1992). In particular, for a meander bend developed by lateral expansion, the process of neck tightening can also induce increased deposition of finer-grained facies on adjacent meander bends. The model defines a threshold of sinuosity/maturity beyond which the sand-prone facies association changes toward an association dominated by finer-grained facies.

Rule set 2: Mud-prone areas associated with downstream-translating bars. Previous studies have demonstrated how counter-point bars may develop when the apex of a meander bend migrates in the down-valley direction, and associated bar forms undertake growth via downstream translation (Burge and Smith, 1999; Ghinassi and Ielpi, 2015; Ghinassi et al., 2016; Jackson, 1976; Nicoll and Hickin, 2010). Notably, this is known to occur in response to the following situations: (1) confinement of a fluvial system within a valley (Ghinassi and Ielpi, 2015); (2) confinement by the presence of deposits that are themselves resistant to erosion, such as mud-prone abandoned channel fills (Labrecque et al., 2011; Smith et al., 2009); and (3) confinement or redirection of a fluvial path by the action of local tectonics (Ghinassi et al., 2014). In contrast to expansional point-bar deposits, which exhibit scroll-bar plan-form morphologies that are convex in the direction of bar propagation and which are usually dominated by sand-prone lithofacies, counter-point bar deposits typically preserve concave-shaped plan-form patterns that comprise mud- or silt-prone lithofacies (Smith et al., 2009). The finer overall grain size and increased lithological heterogeneity

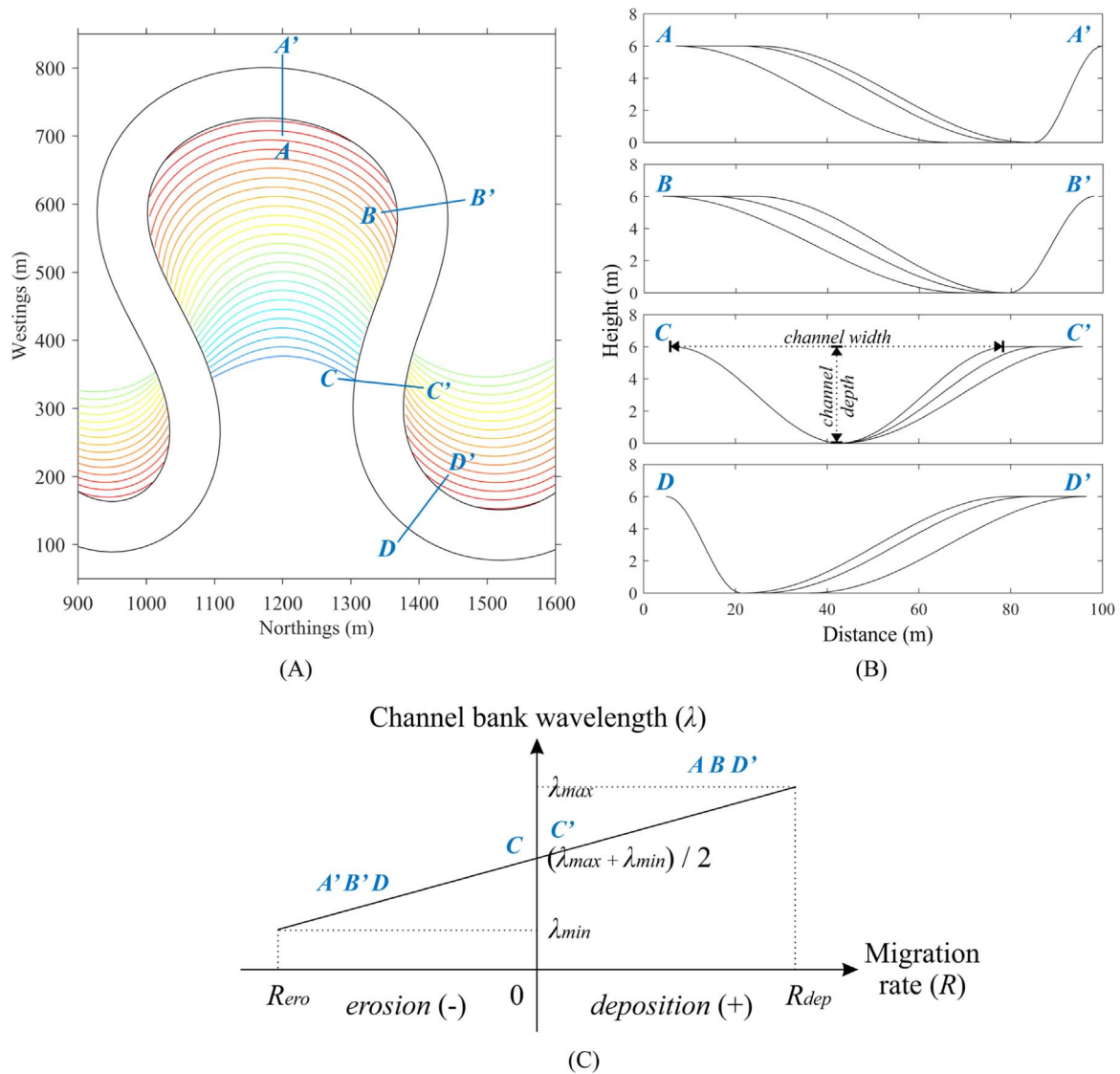


Fig. 7. Algorithm of modelling the shape of channel banks. (A) Plan-view locations of representative cross sections. (B) Channel-bank profiles of representative cross sections. (C) Bank wavelength function. The channel-bank wavelength (λ) that describes the cross-sectional geometry of an accretion surface at a given time is determined by the migration rate (R), following a simple linear relationship, in which λ_{min} and λ_{max} are the minimum and maximum wavelength, i.e., the steepest and gentlest slope that a channel bank can maintain when the bank experiences the largest erosion rate (R_{ero}) and deposition rate (R_{dep}), respectively. Bank A' , B' , and D' are cut banks that experience erosion, whereas bank A , B , and D are inner banks that experience deposition. Bank C and C' are around inflection point of two point bars and exhibit similar shape (i.e., a symmetrical channel cross section).

associated with counter-point-bar deposits is a notable problem in assessing subsurface hydrocarbon reservoir potential (Fustic et al., 2012; Smith et al., 2009).

The transition between a sandy point bar and a muddy counter-point bar occurs at or close to the plan-view inflection or crossover point of a meander bend. To simulate such facies transition, two end-member facies associations are defined to represent typical point-bar deposits and counter-point-bar deposits, respectively. By specifying a transition rate or width, facies associations in the transitional zone at the bend inflection can be interpolated to simulate a gradual change between predefined point-bar deposits and counter-point-bar deposits. The rate at which this change in facies types occurs across the boundary between a “normal” sand-prone point bar and a muddy counter-point bar can be set based on examples observed from natural systems and stored in FAKTS.

Rule set 3: Mud drapes associated with fluvially or tidally induced mud deposition. In fluvial systems, mud drapes form at times of low-

stage flow. Where fluvial systems pass downstream into the so-called fluvial–marine transition zone such that they become influenced by tidal forces (Van Den Berg et al., 2007; Dalrymple and Choi, 2007; Shiers et al., 2014, 2017), mud-drapes on bar fronts commonly form inclined heterolithic strata (IHS). The development of IHS typically takes the form of mud drapes that are deposited periodically on inclined and otherwise sand-prone bar-front surfaces (Nanson, 1980; Thomas et al., 1987), for example in response to daily or semi-diurnal tidal cycles or bi-monthly spring-neap cycles. The distribution of mud drapes can influence significantly the internal lithological heterogeneity of point-bar elements, and therefore exerts a primary influence on fluid-flow pathways in subsurface reservoirs and aquifers composed of such deposits (Labrecque et al., 2011).

Mud draping on bar fronts is modelled using a stochastic approach that allows for control of the frequency and the thickness of these fine-grained deposits. Thick mud drapes typically reflect low-frequency events, such as major flood events with long recession limbs, whereas thin mud drapes – induced, for example, by tidal modulation of river

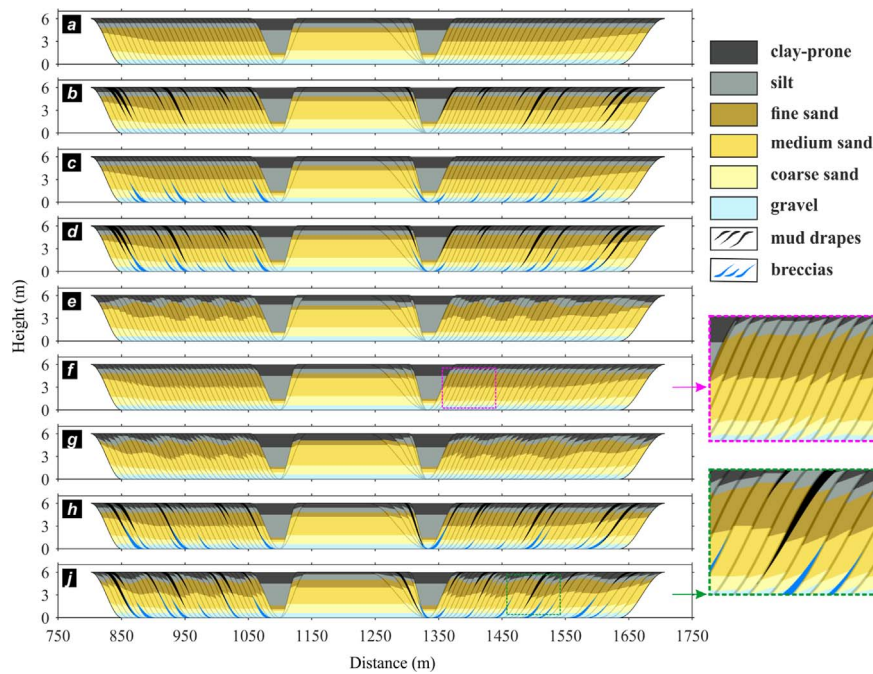


Fig. 8. Examples of modelled cross sections with different lithological characteristics: (a) basic lithological arrangement with fining-upward trend; (b) cross section with mud drapes; (c) cross section with basal breccias; (d) cross section with mud drapes and basal breccias that are nested with each other; (e) cross section with randomised facies components; (f) cross section with inter-digitated facies bounding surfaces; (g) cross section with randomised facies components and inter-digitated facies bounding surfaces; (h) cross section with nested mud drapes and breccias, and inter-digitated facies bounding surfaces; and (j) cross section with nested mud drapes and breccias, randomised facies components, and inter-digitated facies bounding surfaces. Enlarged views on the lower right highlight bed-dipping changes of facies bounding surfaces. Note vertical exaggeration. (For interpretation of the references to color in this figure legend, the reader is referred to the web version of this article).

flow – are likely to be deposited more frequently. By default, within the model, the occurrence of mud drapes in different thicknesses follows a truncated Gaussian distribution (probability density function) defined by the minimum and maximum values and a standard deviation. Different distribution curves can also be defined to match observations from natural systems based on outputs from FAKTS (Colombera et al.,

2012, 2013). Different thicknesses of mud drapes can be nested to represent interactions of multiple sedimentary processes that occur at various spatial and temporal scales (Fig. 9). The pinch-out position of mud drapes on a bar front can also vary either systematically or randomly to simulate the occurrence of mud drapes observed in natural systems (cf. Labrecque et al., 2011). Thus, it is possible to

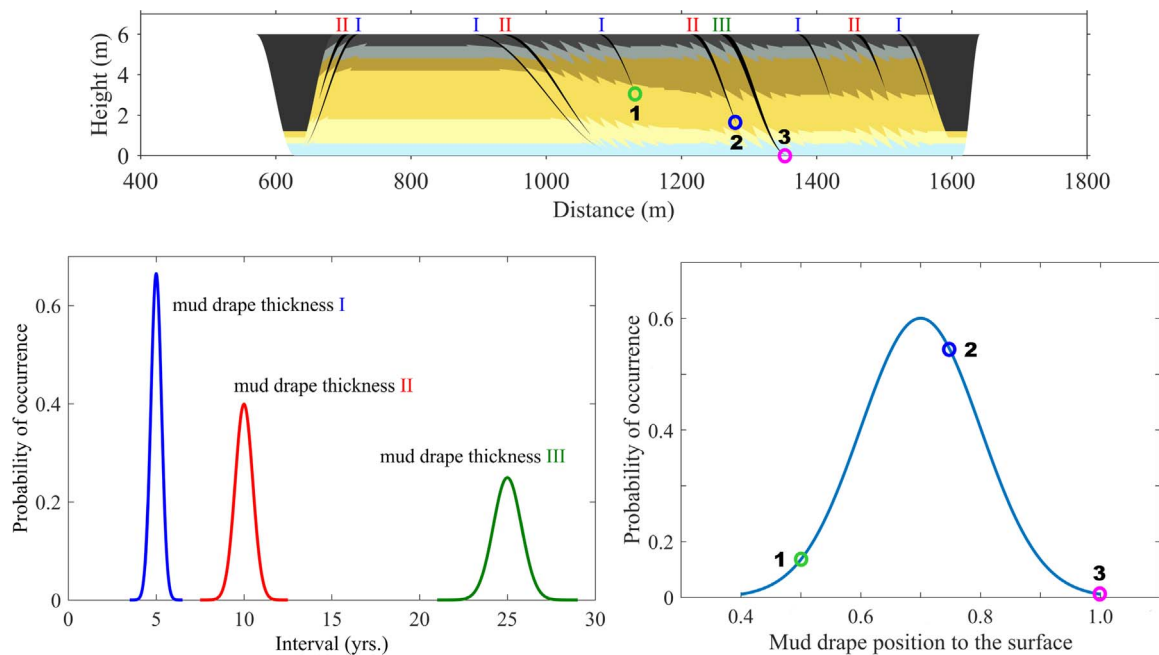


Fig. 9. Examples of modelling multiple-scale mud drapes with three different thicknesses (I, II and III) that are controlled by their respective probability curves of occurrence. The vertical position of the frontal end where mud drapes extend on a bar is also modelled using a Gaussian distribution curve specified by users; three examples are shown in circles. (For interpretation of the references to color in this figure legend, the reader is referred to the web version of this article).

model the coexistence of some mud drapes that extend over the full thickness of bar fronts in combination with other mud drapes that are confined to just the upper-most parts (cross sections *b*, *h* & *j* in Fig. 8).

Rule set 4: Episodic accumulation of gravel lags in channel bases arising from bank collapse in the aftermath of flood events. Collapse of cut banks induced by strong erosion commonly releases pebble-grade intraclasts, which are transported locally in the channel thalweg before being deposited on the lower parts of the accreting channel bank, for example after flood events. Gravel lags can be modelled at different spatio-temporal scales with different thicknesses based on associated probability distribution curves (cross sections *c*, *d* and *j* in Fig. 8). Similarly, the position of gravel lags on inclined bar-front surfaces can also be set to vary stochastically between predefined upper and lower limits.

Rule set 5: Modelling small-scale facies inter-digitation and variability. Two additional controls on facies bounding surfaces enable the model to simulate: (1) different styles of facies inter-digitation in bar accretion packages (cross sections *f*, *g*, *h* and *j* in Fig. 8); and (2) variability in facies proportions, which can be employed to account for inherent randomness in facies arrangements commonly seen in natural systems (cross sections *e*, *g* and *j* in Fig. 8). The inclination of facies bounding surfaces can vary periodically across accretion packages in a bar, from horizontal or gently inclined (the minimum inclination, θ_{inc_min}) to steeply inclined (the maximum inclination, θ_{inc_max}) and back. The proportion of different facies can also vary systematically, linearly and periodically in proportion to the bar thickness (e.g., 2%, from 0+/-2% and back, over the duration of a cycle). Both periods are governed independently by a Gaussian distribution curve, changing between the minimum and maximum times with a specified standard deviation (i.e., a truncated probability distribution func-

tion). More complex distributions can furthermore be defined, as appropriate.

3. Application: Jurassic Scalby Formation, England

Here we demonstrate how to employ real-world data from the literature, from field studies, or from FAKTS (Colombera et al., 2013), to define inputs into PB-SAND. Importantly, we also demonstrate how the outcome obtained from the model can be used to improve our understanding of the complex 3D sedimentary architecture of point-bar elements, thereby aiding in the reconstruction of the morphological evolution and 3D sedimentary architecture of meandering fluvial successions, more generally.

Exhumed meander-belt deposits exposed to the north of Scarborough (Yorkshire Coast, UK) are part of the middle Jurassic Scalby Formation, Ravenscar Group. This succession allows the examination of architectural elements of fluvial origin in both planform (exposures on a wave-cut platform) and as vertical cliff exposures over an area of approximately 3×0.5 km². The outcropping succession has enabled reconstruction of the sedimentary architecture of point-bar deposits (Ielpi and Ghinassi, 2014).

The fluvial point-bar deposits of the Scalby Formation were interpreted originally by Nami (1976) and Leeder and Nami (1979). The complexity of the succession, which is characterised by multiple storeys of point-bar and overbank elements, was revealed in greater detail by Alexander (1986, 1992). Ielpi and Ghinassi (2014) integrated local field measurements with large-scale, high-resolution remote sensing imagery to define the geometry of distinctive architectural elements in both plan-view and vertical sections. Recently, a depositional model has been proposed that establishes a linkage between bedding geometries, 3D facies distribution, and meander-bend transformation behaviours (Ghinassi and Ielpi, 2015; Ghinassi et al., 2016).

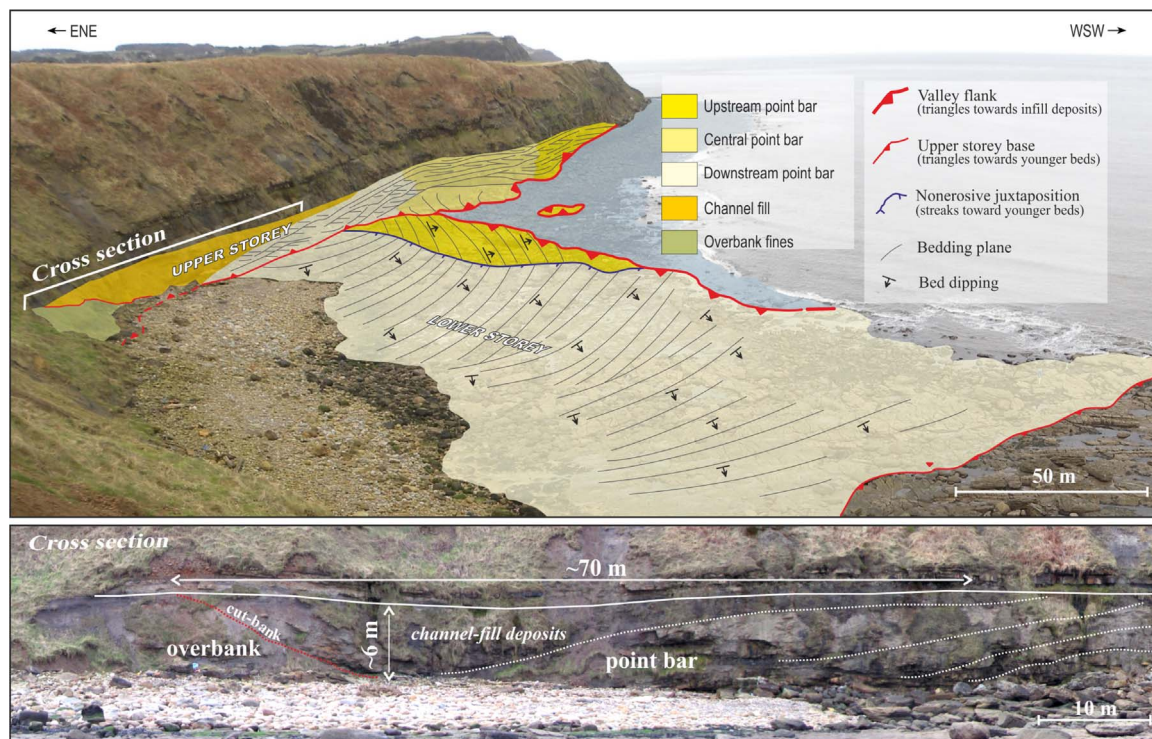


Fig. 10. Planform and cliff expression of the multi-storey bar complex of the Scalby Formation, England (modified after Ielpi and Ghinassi, 2014). There are two different storeys of point-bar deposits: upper and lower. The outcrop of the downstream-migrating point-bar element and related channel-fill deposits is shown in the cross section. (Photos courtesy of Massimiliano Ghinassi ©, (for interpretation of the references to color in this figure legend, the reader is referred to the web version of this article).

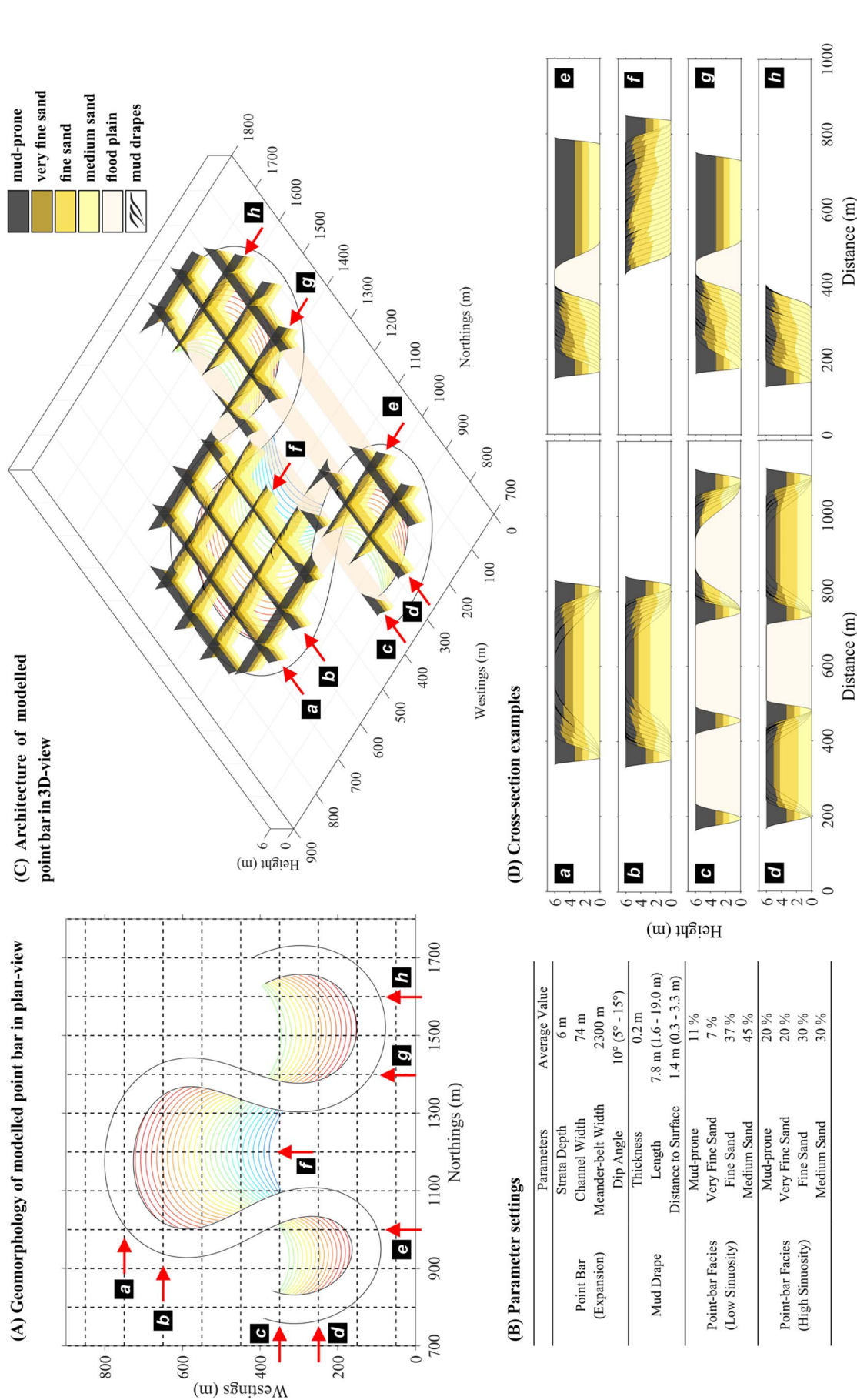
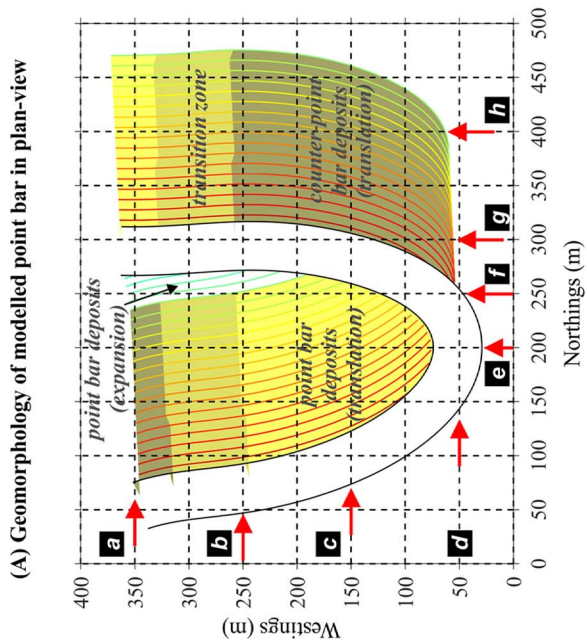
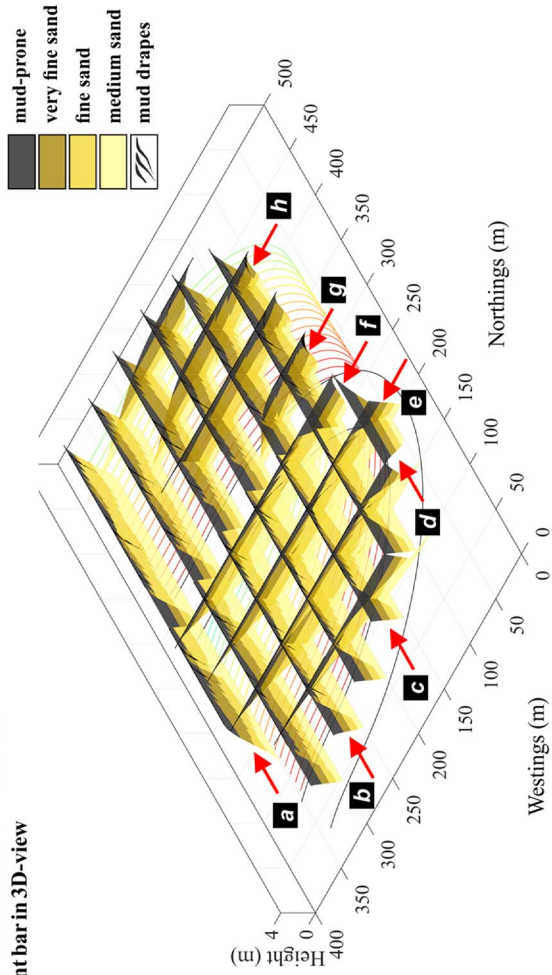


Fig. 11. An example of modelled point bars developed by lateral expansion, comparable to those observed in the upper storey of the Sealby Formation. (For interpretation of the references to color in this figure legend, the reader is referred to the web version of this article).



(A) Geomorphology of modelled point bar in plan-view



(C) Architecture of modelled point bar in 3D-view

(B) Parameter settings

Parameters	Average Value
Point Bar (Downstream Translation)	Strata Depth: 4 m Channel Width: 45 m Meander-belt Width: 350 m Dip Angle: 10° (5° - 15°)
Mud Drape	Thickness: 0.2 m Length: 7.8 m (1.6 - 19.0 m) Distance to Surface: 1.4 m (0.3 - 3.3 m)
Point-bar Facies (Low Simuosity)	Mud-prone: 11% Very Fine Sand: 7% Fine Sand: 37% Medium Sand: 45%
Counter-point-bar Facies	Mud-prone: 20% Very Fine Sand: 35% Fine Sand: 25% Medium Sand: 20%

(D) Cross-section examples

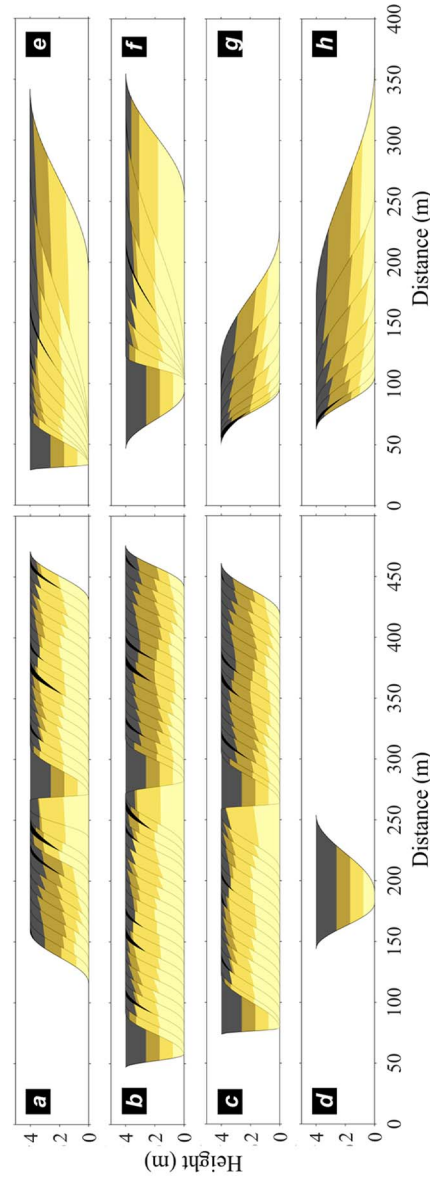


Fig. 12. An example of modelled point bars developed by down-stream translation, comparable to those observed in the lower storey of the Sealby Formation. (For interpretation of the references to color in this figure legend, the reader is referred to the web version of this article).

The exhumed meander plain of the Scalby Formation comprises two storeys of meander-belt deposits as the fill of a valley system (Ielpi and Ghinassi, 2014, Fig. 10). The upper storey is dominated by architectural elements that represent the deposits of expansional point bars in a non-confined setting. By contrast, the lower storey is dominated by architectural elements that represent the deposits of downstream-translating point bars in a laterally confined setting.

We use the PB-SAND model to simulate the internal sedimentary structure and 3D architecture of point-bar elements developed by expansion and translation, respectively. The parameter settings used in the simulations are extracted from FAKTS (Colombera et al., 2013), which comprises field data (Fig. 11B and Fig. 12B) from the earlier outcrop-based studies (Ghinassi and Ielpi, 2015; Ghinassi et al., 2016; Ielpi and Ghinassi, 2014). The modelled point-bar elements generally exhibit fining-upward facies successions: sandy deposits at the bottom, changing upward from medium, to fine, to very fine sandstone; this is overlain by mud-prone facies at the top. Two additional facies types are recognised: mud drapes that occur regularly in the upper part of point-bar deposits, and floodplain deposits that comprise a mixture of silt, clay, and very fine sand and represent the 'background' sediment in which the bar-form elements occur. Although pebble-grade mud clasts are present as deposits in channel fills and erosional reactivation surfaces are present within the preserved point-bar elements, these features are subordinate and hence not included in the simulations.

Lateral accretion beds dip toward the abandoned channel-fill at 5° to 15° (10° on average). Detailed parameter settings and modelling examples of expansion and downstream-translation point-bar elements are depicted in Figs. 11 and 12, respectively. These variables are consistent with relationships documented from other natural examples (cf. Carlston, 1965; Fielding and Crane, 1987; Leeder, 1973; Leopold and Wolman, 1960; Lorenz et al., 1985). Features of modelled point-bar elements are of comparable scale to the fluvial exposures, and modelled internal architectures exhibit similar geometries to those documented by Ielpi and Ghinassi (2014). Compared with high-sinuosity point bars formed by expansion, point bars developed by down-stream translation tend to be relatively narrow due to the inability of the system to expand via lateral-accretion processes (Figs. 11 and 12). Detailed comparisons of PB-SAND modelling outcome with field observations and facies models are presented in Appendix B.

The modelled point-bar succession highlights the 3D stratigraphic significance of several important observations derived from outcrop measurements; the model output portrays the predicted 3D sedimentary architecture of the elements in significantly greater detail than what can be elucidated from outcrop observations alone. Modelling results in Figs. 11 and 12 demonstrate how different migration styles and morphological evolution behaviours of meander bends result in spatial heterogeneity at both the facies and the element scales. Characteristics of preserved bar deposits are also further exemplified in Video 2 [supplemental].

Supplementary material related to this article can be found online at <http://dx.doi.org/10.1016/j.cageo.2017.04.012>.

4. Discussion

Facies models are the abstraction or summary of case examples from preserved modern and ancient successions in specific sedimentary environments (Miall, 1996; Reading, 2001; Walker, 2006). However, existing qualitative facies models are limited in their ability to account for complex facies inter-relationships that are known to occur in 3D, chiefly because known real-world case examples do not usually permit analysis of such 3D relationships. In particular, ancient successions preserved in the rock record are highly fragmentary, and

interpretations are likely biased due to selective preservation of certain parts of successions. One solution to the 'data gap' that arises from incomplete field-derived data sets is the adoption of a numerical modelling approach, whereby limited knowledge from natural systems coupled with predictive understanding of how natural systems evolve over time and space can be used to predict the 3D architecture of sedimentary elements at different scales. Such a modelling approach provides a linkage between local outcrop measurements and large-scale sedimentary architecture; it allows assessment of possible scenarios depicted in traditional qualitative facies models. Furthermore, a numerical modelling approach importantly allows exploration of potential alternatives beyond traditional facies models, possibly for examples where no known natural case study yet exists (Bridge, 1975; Willis and Tang, 2010). Given that preserved bar deposits are fragmentary and because orientations of lateral-accretion bed-sets observed in the field are likely oblique to the trend of the original channels, it is not necessarily straightforward to reconstruct the original channel geometry (true bedding dip) that is parallel to the bar-migration direction or orthogonal to the flow direction from the cross sections. Meanwhile, common limitations are also imposed by the scarcity of representative vertical sections exposed in the field. These issues can be addressed by testing multiple scenarios using PB-SAND and comparing modelling outcomes with outcrop and seismic data. The 3D realisation of modelling outputs can also improve understanding and interpretation of depositional systems compared to analysis of 2D outcrops and exposures alone.

PB-SAND allows exploration of sensitivities of different parameters and the extent to which they influence the sedimentary patterns and meander-bend transformation behaviours in different depositional systems. The statistical and stochastic components in the model, in particular, enable investigation of the effects of intrinsic variability within a system on the possible range of stratal architectures.

This study focuses on the numerical stratigraphic modelling of the geometry and internal facies distribution of individual point-bar elements that are formed by different styles of meander-bend transformations, and the shape of meanders in plan-view cannot be simply assumed to follow any certain wavelength assumption. We herein use bar positions at particular times that can be fully defined by users based on available datasets (e.g., Ielpi and Ghinassi, 2014) to control the evolution of point bars in plan-view. This method allows for considerable flexibility in modelling complicated point-bar geometries. Bed dips in the model change progressively, systematically and realistically around meander bends with channels possessing a symmetrical cross-sectional shape around inflections of a meander and a strong asymmetrical shape at the apex. The maximum channel depth is modelled equal to bar thickness because the channel scour depth does not change significantly around a single meander. This enables high computational efficiency.

In the examples presented, the rules that describe facies patterns and stratal trends are kept simple for the purpose of demonstration and based on the relatively simple sedimentary architectures present in the selected case studies. However, different facies patterns can be defined, as required, based on observations from other natural examples. Although simulations require parameterisation with sedimentological data in sufficient quantity and quality, PB-SAND serves as a tool to explore possible scenarios using available datasets from suitable analogues. The facies associations of representative bar locations can also be conditioned to well or seismic data. Additionally, PB-SAND can be employed to model the style of stratification and distribution of lithofacies arising as a consequence of (1) the partial overprinting of multiple point-bar elements that form laterally amalgamated channel and point-bar belts and complexes, and (2) the vertical stacking and partial overprinting of point-bar elements as a function of on-going accumulation in subsiding basins where accommodation is progres-

sively generated. Analysis of such amalgamation and stacking types will be the focus of future work.

Vector outputs of PB-SAND can be rasterised as 3D grids in the GSLIB format (Deutsch and Journel, 1992). These geo-cellular grids can be used for the following purposes: (1) as templates for flow-based upscaling applied to highly heterogeneous reservoirs (cf. Nordahl et al., 2014); (2) to study the sensitivity of static and dynamic connectivity of meander-belt reservoirs or aquifers to different types of sedimentary heterogeneity (cf. Willis and Tang, 2010); and (3) as input training images for Multiple-Point geo-Statistics (MPS) modelling tools which are widely used in the hydrocarbon industry because of their ability to model complex geometries and yet honour well data (Hu and Chugunova, 2008; Strebelle and Levy, 2008). The application of PB-SAND to the generation of training images can be customised with respect to the types of facies categories that can be included. Upscaling can then be performed to ensure the presence of certain types of heterogeneity in the domain. The ability to capture heterogeneity in the gridded domain relies on a combination of upscaling and post-processing techniques. PB-SAND permits modelling consecutive meander loops or channel belts consisting of amalgamated bars and channel fills. The ability to model repeated patterns is desirable to ensure that stationarity is achieved when using the modelling outputs as MPS training images.

5. Conclusions

The PB-SAND model introduced in this study is able to predict the three-dimensional sedimentary architecture arising from different meander-bend transformations at varying temporal and spatial scales. By comparing modelling results with facies descriptions of the observed stratigraphic record of different types of meandering fluvial

deposits, we have demonstrated that PB-SAND is robust in modelling facies-distribution trends without compromising small-scale details. The modelling outcome enforces our general understanding of distinct bedding geometries and sedimentary structures formed by downstream-translating point-bar elements, as opposed to expansional point-bar elements. High computational efficiency permits multiple model runs in a timely manner (5–60 s for a single point-bar simulation on a standard PC; several minutes for more complex scenarios involving multiple point bars), thereby allowing investigation of multiple scenarios by varying controlling parameters systematically, both spatially and temporally, to reconstruct a variety of meander morphologies, and predict potential vertical and lateral changes in sedimentary architecture and lithology in different geological settings. Furthermore, the approach permits exploration of variations and inherent uncertainties, as well as assessment of the likely range of heterogeneity present in sub-surface bodies that serve as repositories for minerals of economic value, hydrocarbons and groundwater. PB-SAND can also be applied to model the overprinting of multiple point-bar elements, and the stacking and associated connectivity variation of channel belts in response to changes in the avulsion frequency and the subsidence rate.

Acknowledgements

We thank Nexen Energy ULC, Canada for provision of financial support of this project. Massimiliano Ghinassi, Alessandro Ielpi, two anonymous reviewers, and the journal editorial team, Editor-in-Chief, Gregoire Mariethoz, and Associate Editor, Pauline Collon are thanked for their valuable comments and suggestions, which have greatly improved the manuscript.

Appendix A

See Fig. A.1.

Modelling Inputs

<p>single point bar</p> <ul style="list-style-type: none"> point bar transformation style coordinates of bar positions at three key times (x, y) migration rates ($m\ yr^{-1}$) or bar numbers ($\#\ m^{-1}$) between key times number of controlling point for each bar position river width (m) neck cutoff threshold (m) <p>channel asymmetry and shape of inclined accretion surfaces</p> <ul style="list-style-type: none"> river width (m) bar depth (m) dip angle ($^{\circ}$) maximum deposition rate of inner bank ($m\ yr^{-1}$) maximum erosion rate of cut bank ($m\ yr^{-1}$) maximum wavelength of inclined accretion surface (m) minimum wavelength of erodible slope (m) <p>location of cross sections</p> <ul style="list-style-type: none"> cross section area <ul style="list-style-type: none"> width (m) length (m) coordinates of centre (x, y) degree of clockwise rotation ($^{\circ}$) resolutions of cross sections in width (m) and length (m) <p>facies associations</p> <ul style="list-style-type: none"> point bar transformation style facies types proportions of different facies at representative point-bar locations <ul style="list-style-type: none"> early stage expansional point bar mature stage and high sinuosity expansional point bar transitional zone between early and later stages of expansional point bar counter-point bar by downstream translation transitional zone between point bar and counter-point bar apex portion by translation and rotation proportions of different facies in abandoned channels <p>shape of facies bounding surfaces</p> <ul style="list-style-type: none"> inclination for each bounding surface <ul style="list-style-type: none"> minimum and maximum degree of inclination ($^{\circ}$) minimum and maximum years of a cycle (m) shape factor of Gaussian distribution curve for cycling years disorder and randomness level for each bounding surface <ul style="list-style-type: none"> disorder level, in percentage of to bar depth minimum and maximum years of a cycle (m) shape factor of Gaussian distribution curve for cycling years 	<p>multiple point bars</p> <ul style="list-style-type: none"> percentage of different bar transformation styles orientation distribution curve ($^{\circ}$, unimodal or bimodal) size distribution curve point bar longevity control (time or cut-off) point bar density distribution in a channel belt width of channel belt (m) spatial distribution curve of channel belts avulsion frequency of channel belts (yrs) spatial change of subsidence rate, e.g., faults ($m\ yr^{-1}$) tectonic boundaries if existing <p>mud drapes</p> <ul style="list-style-type: none"> probability distribution curves of 1-3 different levels of mud drapes <ul style="list-style-type: none"> thickness (m) minimum occurrence interval (yrs) maximum occurrence interval (yrs) shape factor of Gaussian distribution curve for interval position of mud drapes on bar front <ul style="list-style-type: none"> upper boundary of mud drape front relative to bar depth lower boundary of mud drape front relative to bar depth shape factor of Gaussian distribution curve for position continuity of mud drapes in cross sections <ul style="list-style-type: none"> maximum numbers (1-3) of gaps within a mud drape size of gap relative to bar depth upper boundary of the gap position relative to bar depth lower boundary of the gap position relative to bar depth probability of occurrence of 1-3 gaps shape factor of Gaussian distribution curve for gap position continuity of mud drapes in plan view <ul style="list-style-type: none"> minimum length of mud drapes (m) maximum length of mud drapes (m) shape factor of Gaussian distribution curve for length minimum length of spacing (m) maximum length of spacing (m) shape factor of Gaussian distribution curve for spacing <p>conglomerates or breccias</p> <ul style="list-style-type: none"> probability distribution curves of 1-3 different levels of conglomerates or breccias <ul style="list-style-type: none"> thickness (m) minimum occurrence interval (yrs) maximum occurrence interval (yrs) shape factor of Gaussian distribution curve for interval uppermost position of conglomerates or breccias on bar front <ul style="list-style-type: none"> upper boundary relative to bar depth lower boundary relative to bar depth shape factor of Gaussian distribution curve for position
---	--

Modelling Outputs

<ul style="list-style-type: none"> high resolution plan-view morphology facies distribution in 3D bounding surface geometries (2nd order) mud drapes at different scales (3rd order) multiple point-bar elements in a meander belt multiple meander belts 	<ul style="list-style-type: none"> stacking patterns and connectivity change caused by different subsidence rates and avulsion rates sensitivity of parameter controls cross sections training images for MPS 3D fence diagrams ACSII txt. format output files
---	---

Fig. A.1. Inputs and outputs of PB-SAND.

Appendix B

Modelled cross sections *a* and *f* in Fig. 11, and cross sections *b* and *e* in Fig. 12 are, both geometrically and morphologically, comparable with cross sections *A-A'*, *B-B'*, *C-C'* and *D-D'* of the facies model in Fig. 18 by Ielpi and Ghinassi (2014), respectively. For cross sections parallel to the channel-belt axis, the dip of accretion surfaces within the expansional point bar decreases progressively from the upstream- to central-bar portions, and then increases through the downstream-bar portion, whereas the dip of accretion surfaces within the translating point bar does not show apparent change (e.g., cross section *a* in Fig. 11 vs. cross section *b* in Fig. 12). In contrast, for cross sections transverse to the channel-belt axis, the

dip of accretion surfaces is essentially maintained within the expansional point bar, whereas the dip changes rapidly within the translating point bar (e.g., cross section *f* in Fig. 11 vs. cross section *e* in Fig. 12).

As the translating point bar migrated downstream, the upstream-bar deposits were progressively reworked and eroded. The point-bar deposits developed by expansion at the early stage (see Fig. 12A) have been almost completely eroded, and downstream-bar deposits are preferentially preserved. Upstream-bar deposits of the expansional point bar, by comparison, are for the most part well preserved, especially for higher sinuosity meander-bend deposits that occur further away from the axis of the channel belt. This is consistent with field observations reporting that translating point bars exhibit systematic erosion and sediment bypass (Ghinassi and Ielpi, 2015; Ghinassi et al., 2016, 2014; Ielpi and Ghinassi, 2014; Smith et al., 2011; Smith et al., 2009).

The morpho-dynamics of meander-bend transformations also lead to spatial variations in facies assemblages. As a meander-bend migrates laterally, an increase in sinuosity and the associated bend-tightening encourages the deposition of finer grained facies (Jackson, 1976), which is replicated in the modelled point bar in Fig. 11. For example, mud-prone and very fine sand facies increase, in general, from the central portion toward the abandoned channel either upstream or downstream, as shown in cross sections *b* & *d*. Similarly, finer grained facies increases in the transverse direction, away from the channel-belt axis; see cross sections *f* & *h*. Meanwhile, given that lateral barform development is confined and limited by non-erosional strata, downstream-translating meanders tend to develop as sand-prone point bars and mud-prone counter-point bars. The zone of transition between these sand-prone and mud-prone deposits occurs close to the inflections of the meander-bends (Jackson, 1976; Labrecque et al., 2011; Smith et al., 2011, 2009). As observed in the modelled example in Fig. 12, cross section *a* passes through the mud-prone and very-fine-sand-dominated counter-point-bar deposits, then through point-bar deposits preserved from the earlier expansional phase of bar development, and crosses channel-fills, finally reaching the fine- and medium-sand dominated point-bar deposits. Mud drapes in both examples are limited to the top of inclined bar surfaces (Figs. 11 and 12), akin to field observations in the Scalby Formation (Ghinassi et al., 2016, 2014; Ielpi and Ghinassi, 2014).

References

- Alexander, J., 1986. Sedimentary and tectonic controls of alluvial facies distribution: Middle Jurassic, Yorkshire and the North Sea Basins and the Holocene, SW Montana, USA. The University of Leeds, Leeds, UK, Ph.D. thesis.
- Alexander, J., 1992. Nature and origin of a laterally extensive alluvial sandstone body in the Middle Jurassic Scalby Formation. *J. Geol. Soc.* 149, 431–441.
- Allen, J.R.L., 1970. Studies in fluvial sedimentation - a comparison of fining-upwards cyclothem, with special reference to coarse-member composition and interpretation. *J. Sediment. Petrol.* 40, 298–323.
- Brice, J.C., 1974. Evolution of meander loops. *Geol. Soc. Am. Bull.* 85, 581–586.
- Bridge, J.S., 1975. Computer-simulation of sedimentation in meandering streams. *Sedimentology* 22, 3–43.
- Bridge, J.S., 2003. Rivers and Floodplains: Forms, Processes, and Sedimentary Record: Malden. Blackwell Publishing.
- Bridge, J.S., Alexander, J.A.N., Collier, R.E.L., Gawthorpe, R.L., Jarvis, J., 1995. Ground-penetrating radar and coring used to study the large-scale structure of point-bar deposits in three dimensions. *Sedimentology* 42, 839–852.
- Brownlie, W.R., 1983. Flow depth in sand-bed channels. *J. Hydraul. Eng.-Asce* 109, 959–990.
- Burge, L.M., Smith, D.G., 1999. Confined meandering river eddy accretions: sedimentology, channel geometry and depositional processes. *Spec. Publ. int. Ass. Sediment.* 28, 113–130.
- Carlston, C.W., 1965. The relationship of free meander geometry to stream discharge and its geomorphic implications. *Am. J. Sci.* 263, 864–885.
- Colombera, L., Mountney, N.P., McCaffrey, W.D., 2012. A relational database for the digitization of fluvial architecture: concepts and example applications. *Petr. Geosci.* 18, 129–140.
- Colombera, L., Mountney, N.P., McCaffrey, W.D., 2013. A quantitative approach to fluvial facies models: Methods and example results. *Sedimentology* 60, 1526–1558.
- Colombera, L., Mountney, N.P., Russell, C.E., Shiers, M.N., McCaffrey, W.D., 2017. Geometry and compartmentalization of fluvial meander-belt reservoirs at the barform scale: quantitative insight from outcrop, modern and subsurface analogues. *Mar. Petrol. Geol.* 82, 35–55.
- Constantine, J.A., Dunne, T., 2008. Meander cutoff and the controls on the production of oxbow lakes. *Geology* 36, 23–26.
- Dalrymple, R.W., Choi, K., 2007. Morphologic and facies trends through the fluvial-marine transition in tide-dominated depositional systems: a schematic framework for environmental and sequence-stratigraphic interpretation. *Earth-Sci. Rev.* 81, 135–174.
- Daniel, J.F., 1971. Channel movement of meandering Indiana streams. *U.S. Geol. Surv. Prof. Pap.* 732A, 1–18.
- Deutsch, C.V., Journel, A.G., 1992. Geostatistical software library and user's guide. Oxford University Press, New York, 340.
- Dey, S., 2014. Fluvial Processes: Meandering and Braiding, *Fluvial Hydrodynamics: Hydrodynamic and Sediment Transport Phenomena*. Springer Berlin Heidelberg, Berlin, Heidelberg, 529–562.
- Durkin, P.R., 2016. The evolution of fluvial meander belts and their product in the rock record Ph.D. thesis. University of Calgary, Calgary, Alberta, 245.
- Edwards, M.B., Eriksson, K.A., Kier, R.S., 1983. Paleochannel geometry and flow patterns determined from exhumed Permian point bars in north-central Texas. *J. Sediment. Petrol.* 53, 1261–1270.
- Fielding, C.R., Crane, R.C., 1987. An application of statistical modelling to the prediction of hydrocarbon recovery factors in fluvial reservoir sequences, recent developments in fluvial sedimentology. *SEPM Soc. Sediment. Geol.* 39, 321–327.
- Fisk, H.N., 1944. Geological investigation of the alluvial valley of the lower Mississippi River. U.S. Department of the Army, Mississippi River Commission, 1–78.
- Foix, N., Allard, J.O., Paredes, J.M., Giacosa, R.E., 2012. Fluvial styles, paleohydrology and modern analogues of an exhumed, Cretaceous fluvial system: Cerro Bacino Formation, Cañadón Asfalto Basin, Argentina. *Cretac. Res.* 34, 298–307.
- Fustic, M., Hubbard, S.M., Spencer, R., Smith, D.G., Leckie, D.A., Bennett, B., Larter, S., 2012. Recognition of down-valley translation in tidally influenced meandering fluvial deposits, Athabasca Oil Sands (Cretaceous), Alberta, Canada. *Mar. Petrol. Geol.* 29, 219–232.
- Ghinassi, M., Ielpi, A., 2015. Stratigraphic architecture and morphodynamics of downstream-migrating fluvial point bars (Jurassic Scalby Formation, U.K.). *J. Sediment. Res.* 85, 1123–1137.
- Ghinassi, M., Ielpi, A., Aldinucci, M., Fustic, M., 2016. Downstream-migrating fluvial point bars in the rock record. *Sediment. Geol.* 334, 66–96.
- Ghinassi, M., Nemec, W., Aldinucci, M., Nehyba, S., Özaksoy, V., Fidinelli, F., 2014. Planform evolution of ancient meandering rivers reconstructed from longitudinal outcrop sections. *Sedimentology* 61, 952–977.
- Hassanpour, M.M., Pycz, M.J., Deutsch, C.V., 2013. Improved geostatistical models of inclined heterolithic strata for McMurray Formation, Alberta, Canada. *AAPG Bull.* 97, 1209–1224.
- Hickin, R.G., 1974. The development of meanders in natural river-channels. *Am. J. Sci.* 274, 414–442.
- Hickin E.J., 1984. Vegetation and river channel dynamics: Canadian Geographer / *Le Géographe canadien*, 28, 111–126.
- Hooke, J., 2003. River meander behaviour and instability: a framework for analysis. *Trans. Inst. Br. Geogr.* 28, 238–253.
- Hooke, J.M., Yorke, L., 2011. Channel bar dynamics on multi-decadal timescales in an active meandering river. *Earth Surf. Process. Landf.* 36, 1910–1928.
- Hu, L.Y., Chugunova, T., 2008. Multiple-point geostatistics for modeling subsurface heterogeneity: a comprehensive review. *Water Resour. Res.* 44, W11413.
- Ielpi, A., Ghinassi, M., 2014. Planform architecture, stratigraphic signature and morphodynamics of an exhumed Jurassic meander plain (Scalby Formation, Yorkshire, UK). *Sedimentology* 61, 1923–1960.
- Jackson, R.G., 1976. Depositional model of point bars in the lower Wabash River. *J. Sediment. Res.* 46, 579–594.
- Kostic, B., Aigner, T., 2007. Sedimentary architecture and 3D ground-penetrating radar analysis of gravelly meandering river deposits (Neckar Valley, SW Germany). *Sedimentology* 54, 789–808.
- Labrecque, P.A., Hubbard, S.M., Jensen, J.L., Nielsen, H., 2011. Sedimentology and stratigraphic architecture of a point bar deposit, Lower Cretaceous McMurray Formation, Alberta, Canada. *Bull. Can. Petrol. Geol.* 59, 147–171.
- Leeder, M.R., 1973. Fluvial fining-upwards cycles and the magnitude of palaeochannels. *Geol. Mag.* 110, 265–276.
- Leeder M.R., Nami M., 1979. Sedimentary models for the non-marine Scalby Formation (Middle Jurassic) and evidence for Late Bajocian/Bathonian uplift of the Yorkshire Basin. *Proceedings of the Yorkshire Geological and Polytechnic Society*, 42, 461–482.
- Leopold, L.B., Wolman, M.G., 1960. River Meanders 71. *Geological Society of America Bulletin*, 789–794.
- Lorenz, J.C., Heinze, D.M., Clark, J.A., Searls, C.A., 1985. Determination of widths of meander-belt sandstone reservoirs from vertical downhole data, Mesaverde Group, Piceance Creek Basin, Colorado 69. *AAPG Bulletin*, 710–721.
- Makasse, B., Weerts, H.J.T., 2005. Muddy lateral accretion and low stream power in a sub-recent confined channel belt, Rhine-Meuse delta, central Netherlands. *Sedimentology* 52, 651–668.
- Miall, A.D., 1994. Reconstructing fluvial macroform architecture from two-dimensional outcrops: examples from the Castlegate Sandstone, Book Cliffs, Utah. *J. Sediment. Res.* 64, 146–158.
- Miall, A.D., 1996. *The Geology of Fluvial Deposits*. Springer-Verlag, New York.
- Motta, D., Abad, J.D., Langendoen, E.J., Garcia, M.H., 2012. A simplified 2D model for meander migration with physically-based bank evolution. *Geomorphology* 163–164, 10–25.
- Musial, G., Reynaud, J.-Y., Gingras, M.K., Fénéès, H., Labourdette, R., Parize, O., 2012.

- Subsurface and outcrop characterization of large tidally influenced point bars of the Cretaceous McMurray Formation (Alberta, Canada). *Sediment. Geol.* 279, 156–172.
- Nami, M., 1976. An exhumed Jurassic meander belt from Yorkshire, England. *Geol. Mag.* 113, 47–52.
- Nanson, G.C., 1980. Point bar and floodplain formation of the meandering Beatton River, northeastern British Columbia, Canada. *Sedimentology* 27, 3–29.
- Nanson, G.C., Croke, J.C., 1992. A genetic classification of floodplains. *Geomorphology* 4, 459–486.
- Nanson, G.C., Hickin, E.J., 1983. Channel migration and incision on the Beatton River. *J. Hydraul. Eng.* 109, 327–337.
- Nicoll, T.J., Hickin, E.J., 2010. Planform geometry and channel migration of confined meandering rivers on the Canadian prairies. *Geomorphology* 116, 37–47.
- Nordahl, K., Messina, C., Berland, H., Rustad, A.B., Rimstad, E., 2014. Impact of multiscale modelling on predicted porosity and permeability distributions in the fluvial deposits of the Upper Lunde Member (Snorre Field, Norwegian Continental Shelf). In: Martinius, A.W., Howell, J.A., Good, T.R. (Eds.), *Sediment-body Geometry and Heterogeneity: Analogue Studies for Modelling the Subsurface*. 387. Geological Society Special Publications, London, 85–109.
- Piet, L.J.M., 1992. *Sedimentology of point bars and oxbow-fills*. University of Calgary, Alberta, Canada, 107, M.Sc. Thesis.
- Reading, H.G., 2001. Clastic facies models, a personal perspective. *Bulletin of the Geological Society of Denmark* 48, 101–115.
- Rubin, D.M., 1987. Cross-Bedding, Bedforms, and Paleocurrents. *Society of Economic Paleontologists and Mineralogists*, Tulsa, 187.
- Savitzky, A., Golay, M.J.E., 1964. Smoothing and differentiation of data by simplified least squares procedures. *Anal. Chem.* 36, 1627–1639.
- Schumm, S.A., 1960. The shape of alluvial stream channels in relation to sediment type. *J. Geophys. Res.* 65, 1638–1638.
- Shiers, M.N., Mountney, N.P., Hodgson, D.M., Cobain, S.L., 2014. Depositional controls on tidally influenced fluvial successions, Neslen Formation, Utah, USA. *Sediment. Geol.* 311, 1–16.
- Shiers, M.N., Mountney, N.P., Hodgson, D.M., 2017. Response of a coal-bearing coastal plain succession to marine transgression: Campanian Neslen Formation, Utah, U.S.A. *J. Sediment. Res.* 87, 168–187.
- Slingerland, R., Smith, N.D., 2004. River avulsions and their deposits. *Ann. Rev. Earth Planet. Sci.* 32, 257–285.
- Smith, R.M.H., 1987. Morphology and depositional history of exhumed Permian point bars in the southwestern Karoo, South Africa. *J. Sediment. Petrol.* 57, 19–29.
- Smith, D.G., Hubbard, S.M., Lavigne, J.R., Leckie, D.A., Fustic, M., 2011. Stratigraphy of counter-point-bar and eddy-accretion deposits in low-energy meander belts of the Peace-Athabasca Delta, Northeast Alberta, Canada. In: Davidson, S.K., Leleu, S., North, C.P. (Eds.), *From River to Rock Record: The Preservation of Fluvial Sediments and Their Subsequent Interpretation*. Society for Sedimentary Geology Special Publication, Tulsa, 143–152.
- Smith, D.G., Hubbard, S.M., Leckie, D.A., Fustic, M., 2009. Counter point bar deposits: lithofacies and reservoir significance in the meandering modern Peace River and ancient McMurray Formation, Alberta, Canada. *Sedimentology* 56, 1655–1669.
- Strebelle, S., Levy, M., 2008. Using multiple-point statistics to build geologically realistic reservoir models: theMPS/FDM workflow. In: Robinson, A., Griffiths, P., Price, S., Hegre, J., Muggeridge, A. (Eds.), *The Future of Geological Modelling in Hydrocarbon Development* 309. Geological Society Special Publications, London, 67–74.
- Thomas, R.G., Smith, D.G., Wood, J.M., Visser, J., Calverley-Range, E.A., Koster, E.H., 1987. Inclined heterolithic stratification—terminology, description, interpretation and significance. *Sediment. Geol.* 53, 123–179.
- Van Den Berg, J.H., Boersma, J.R., Van Gelder, A., 2007. Diagnostic sedimentary structures of the fluvial-tidal transition zone ? Evidence from deposits of the Rhine and Meuse. *Neth. J. Geosci. / Geol. en Mijnbouw* 86, 287–306.
- Walker, R.G., 2006. Facies models revisited. In: Posamentier, H.W., Walker, R.G. (Eds.), *Facies Models Revisited*, SEPM Special Publication 84, 1–17.
- Willis, B.J., Tang, H., 2010. Three-dimensional connectivity of point-bar deposits. *Sediment Res* 80, 440–454.
- Wu J.Y., Shi S.M., Feng X., Wu X.X., Du X.L. and Bao Y., 2015. Internal architecture analysis and modeling of point-bar—a case study of P12 formation, X area. In: *Energy and Environmental Engineering*. In: *Proceedings of the 2014 International Conference on Energy and Environmental Engineering (ICEEE 2014)*, September 21–22, 2014, Hong Kong (Vol. 1, p. 149). CRC Press.